ELSEVIER

Coordination Chemistry Reviews
190–192 (1999) 309–330

COORDINATION CHEMISTRY REVIEWS

www.elsevier.com/locate/ccr

Electronic structures of quasi-one-dimensional halogen-bridged Ni^{III} complexes with strong electron-correlations

Masahiro Yamashita [a,*], Toshio Manabe [a], Takuya Kawashima [a], Hiroshi Okamoto [b], Hiroshi Kitagawa [c]

[a] *Graduate School of Human Informatics and PRESTO (JST), Nagoya University, Furocho, Chikusa-ku, Nagoya 464-8601, Japan*

[b] *Department of Applied Physics, The University of Tokyo, Hongo, Bunkyo-ku, Tokyo 113-8656, Japan*

[c] *Japan Advanced Institute of Science and Technology, Ishikawa 923-1292, Japan*

Accepted 17 February 1999

Contents

* Corresponding author. Tel.: +81-52-789-4835; fax: +81-52-789-4808.
E-mail address: yamashit@info.human.nagoya-u.ac.jp (M. Yamashita)

PII: S0010-8545(99)00073-9

Abstract

In the quasi-one-dimensional halogen-bridged metal complexes, the Pt and Pd compounds have charge density wave (CDW) states or the M^{II}–M^{IV} mixed-valence states where the bridging halogens are distorted from the midpoints between neighboring two metal ions due to the stronger electron–phonon interaction. However, Ni compounds have spin density wave (SDW) states or the M^{III} states where the bridging halogens are located at the midpoints between neighboring two metal ions, due to the stronger electron-correlation. These Ni compounds are not Mott-insulators but charge-transfer-insulators. The electronic structures in $[Ni^{III}(chxn)_2X]Y_2$ (chxn = cyclohexanediamine; X = Cl, Br and mixed-halides; Y = Cl, Br, mixed-helides, NO_3, ClO_4 and BF_4) are tuned by substituting the bridging halogens and counteranions. The competition between the SDW states in Ni^{III} sites and the CDW states in Pd^{II}–Pd^{IV} sites in the Ni–Pd mixed-metal compounds, $Ni_{1-x}Pd_x(chxn)_2Br_3$, has been investigated. The Pd^{II}–Pd^{IV} states are approaching the Pd^{III} states with increase of the Ni components in this system due to the stronger electron-correlation in Ni^{III} sites.

Keywords: MX-chains; Spin density wave; Charge density wave; Peierls-Hubbard model

1. Introduction

Recently, low-dimensional compounds have been attracting much attention since they show very interesting physical properties based on the low-dimensional crystal and electronic structures such as Peierls transition, spin-Peierls transition, neutral-ionic transition, charge density wave (CDW) state, spin density wave (SDW) state, superconductivity etc. [1]. Among these compounds, the quasi-one-dimensional halogen-bridged Pt, Pd and Ni mixed-valence compounds (hereafter abbreviated as MX chain compounds) have been extensively investigated for the last 20 years because they show very interesting properties such as dichroic and intense intervalence charge transfer bands, progressive resonance Raman spectra, luminescences with large Stokes shift, midgap absorptions attributable to the solitons and polarons, large third-order nonlinear optical susceptibilities etc. [2–4]. Theoretically speaking, the MX chains are considered as a Peierls–Hubbard system where the electron–phonon interaction (S), the electron transfer (T), the on-site and inter-site Coulomb interactions (U and V, respectively) compete or cooperate with one another as shown in Fig. 1 [5–7]. Originally, the MX chains are considered as one-dimensional metallic states with half-filled d_{z^2} orbitals of the metal ions and the filled p_z orbitals of the bridging halogen ions. However, as is well known, the one-dimensional metallic state is unstable and is subsequently transferred to the insulating state by the electron–phonon interaction (S) or the electron-correlation (U) (Fig. 2). In most Pt and Pd compounds, due to the strong electron–phonon interaction (S), the bridging halogen ions are distorted from the midpoints between the neighboring two metal ions, giving the CDW states or M^{II}–M^{IV} mixed-valence states (...M^{II}...X–M^{IV}–X...M^{II}...). Accordingly, the half-filled metallic bands are

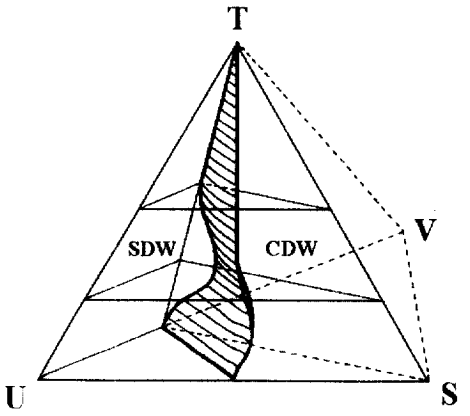

Fig. 1. Phase diagram in the *T*-*U*-*S*-*V* tetrahedron (*T*, electron transfer energy; *U*, on-site Coulomb repulsion energy; *S*, electron-phonon interaction energy; *V*, inter-site Coulomb repulsion energy). The CDW and SDW show the charge density wave state and the spin density wave state, respectively. The shaded plane denotes the phase boundary between these two phases.

split into the occupied valence bands and the unoccupied conduction bands with the finite Peierls gaps. Therefore, these compounds belong to the class II type of the Robin–Day classification for mixed-valence compounds [1]. So far more than 200 compounds of M = Pt and Pd have been synthesized, since the constituents such as metal ions, in-plane ligands, etc. are various and capable of substitution. These compounds are formulated as $[M^{II}(AA)_2][M^{IV}X_2(AA)_2]Y_4$ (abbreviated as $M(AA)_2XY_2$; M^{II}-M^{IV} = Pt^{II}-Pt^{IV}, Pd^{II}-Pd^{IV}, Ni^{II}-Pt^{IV}, Pd^{II}-Pt^{IV}, and Cu^{II}-Pt^{IV}; X = Cl, Br and I; Y = ClO_4, BF_4, PF_6, X, etc.; AA = ethylenediamine(en), cyclohexanediamine(chxn), etc.).

1. The magnitudes of the band gaps can be tuned by varying chemical factors such as M, X, AA, and Y, that is, the physical parameters (*S*, *T*, *U* and *V*) can be tuned by substitution of the chemical factors.
2. The interchain interaction or the dimensionalities of the CDW states can be controlled by using the intra- and inter-chain hydrogen bonds between the aminohydrogens and the counteranions.

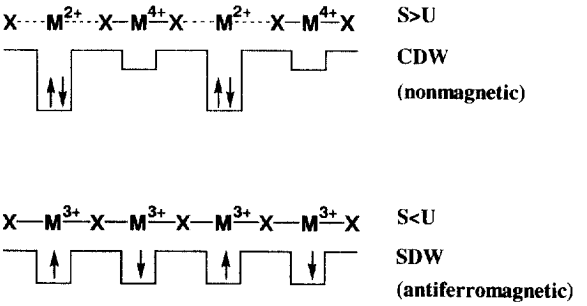

Fig. 2. CDW states (upper) and SDW states (lower), and their spin states for d_{z^2} orbitals of metal ions

3. Single crystals can easily be obtained.

On the other hand, theoretically it was proposed that in the case of the stronger on-site Coulomb interaction (U) compared with the electron–phonon interaction (S), the M^{III} states or SDW states are considered to be more stable, where the bridging halogens are located at the midpoints between the neighboring two metal ions (–X–M^{III}–X–M^{III}–X–). Therefore, these compounds belong to the class III type of the Robin–Day classification for the mixed-valence compounds [1]. Our group succeeded in synthesizing such compounds formulated as $[Ni^{III}(chxn)_2X]Y_2$ (X = Cl, Br and mixed-halides; Y = Cl, Br, mixed-halide, NO_3, ClO_4, etc.), since a Ni ion has the stronger U compared with that of a Pd or Pt ion [8,9]. More recently, we have succeeded in synthesizing the Ni–Pd mixed-metal compounds, where the electron-correlation of the Ni^{II} sites and the electron–phonon interaction of the Pd^{II}–Pd^{IV} sites compete with each other.

While several reviews on Pt and Pd compounds have been published concerning the crystal structures, the resonance Raman spectra, and the dynamics of solitons and polarons [10], no reviews on the Ni compounds have so far been published.

In this review, we will focus on the electronic structures of $[Ni^{III}(chxn)_2X]Y_2$, and the competition between CDW and SDW states in the Ni–Pd mixed-metal compounds, $Ni_{1-x}Pd_x(chxn)_2Br_3$.

2. Electronic structures of $[Ni^{III}(chxn)_2X]Y_2$

2.1. Syntheses of Ni^{III} complexes

Single crystals of $[Ni^{III}(chxn)_2X]X_2$ (X = Cl and Br) were obtained by halogenations of the 2-methoxyethanol solutions of $[Ni^{II}(chxn)_2]X_2$ [8,9]. Single crystals of the mixed-halogen compounds, $Ni(chxn)_2Cl_{2.459}Br_{0.541}$ and $Ni(chxn)_2Cl_{1.28}Br_{1.72}$ were obtained by slow diffusion of Br_2 and Cl_2 into the 2-methoxyethanol solutions of $[Ni(chxn)_2]Cl_2$ and $[Ni(chxn)_2]Br_2$, respectively [11]. Single crystals of $[Ni(chxn)_2X](NO_3)_2$ (X = Cl and Br) were synthesized by an electrochemical method using 2-methoxyethanol solutions of $[Ni(chxn)_2]X_2$ including NH_4NO_3 as an electrolyte [12]. $[Ni(chxn)_2X](ClO_4)_2$ was obtained by halogenation of 70% $HClO_4$ solutions of $[Ni(chxn)_2](ClO_4)_2$ at -10°C. The $[Ni(chxn)_2Cl](BF_4)_2$ was obtained by chlorination of the 40% HBF_4 solution of $Ni(chxn)_2(BF_4)_2$ at -10°C.

2.2. Crystal structures of Ni^{III} complexes

The crystal structures of $[Ni(chxn)_2X]X_2$ (X = Cl and Br), $Ni(chxn)_2Cl_xBr_y$ and $[Ni(chxn)_2X](NO_3)_2$ are isomorphous to one another, and moreover to the mixed-valence compounds $[M^{II}(chxn)_2][M^{IV}(chxn)_2X_2]Y_4$ (M = Pt and Pd; X = Cl, Br and I; Y = X and ClO_4) although the positions of the bridging halogens are different from one another [13]. The chain structure of $[Ni(chxn)_2Br]Br_2$ is shown in Fig. 3. The relevant bond distances of these compounds are listed in Table 1. The four N atoms of two chxn are coordinated to a Ni atom in a planar fashion. The $Ni(chxn)_2$

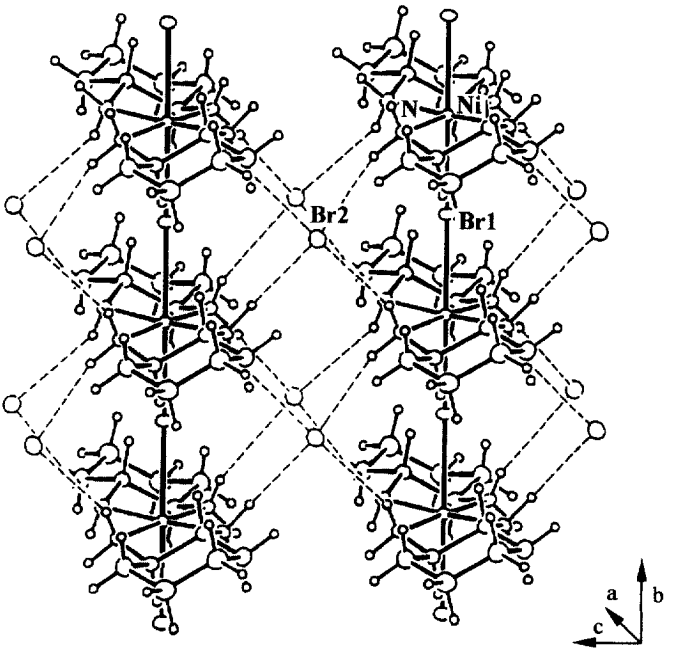

Fig. 3. Crystal structure of $[Ni^{III}(chxn)_2Br]Br_2$. In the crystal, the planar $[Ni^{III}(chxn)_2]$ units are bridged with Br ions, forming the linear chain structures. Each chain is hydrogen-bonded with Br counteranions, forming two-dimensional hydrogen-bond networks.

moieties, lying on special position 222, are bridged by halogen atoms and stacked along the *b*-axis, constructing linear-chain structures. The neighboring $Ni(chxn)_2$ moieties along the chain are linked by the hydrogen bonds between aminohydrogens and counteranions, and moreover, there are hydrogen bonds among the neighboring chains, constructing the two-dimensional hydrogen bond networks parallel to the bc plane. In $Ni(chxn)_2X(NO_3)_2$ (X = Cl and Br), the intra- and inter-chain hydrogen bonds are composed of NH...O...HN and NH...O–N–O...HN systems, respectively. In $Ni(chxn)_2Cl_xBr_y$, the occupancy factors of Cl and Br ions in the bridging and counteranion positions were determined by the

Table 1
Crystal data and relevant bond distances in $[Ni(chxn)_2X]Y_2$ (Å)

	a	*b*	*c*	Ni–X	Ni–N
$Ni(chxn)_2Cl_3$	23.975(5)	4.894(1)	6.913(1)	2.447(1)	1.944(1)
$Ni(chxn)_2Cl_{2.459}Br_{0.541}$	23.901(1)	4.914(1)	6.971(1)	2.457(1)	1.934(2)
$Ni(chxn)_2Cl(NO_3)_2$	22.990(20)	4.982(3)	8.001(5)	2.491(1)	1.927(7)
$Ni(chxn)_2Cl_{1.28}Br_{1.72}$	23.720(2)	5.063(1)	7.189(1)	2.531(1)	1.948(3)
$Ni(chxn)_2B_3$	23.587(5)	5.161(2)	7.121(1)	2.578(1)	1.944(3)
$Ni(chxn)_2Br(NO_3)_2$	22.906(3)	5.213(1)	7.855(1)	2.6065(5)	1.937(4)

full-matrix least-squares refinements. The occupancy factors of Cl and Br at the bridging halogen sites are 0.976 and 0.024 for $Ni(chxn)_2Cl_{2.459}Br_{0.541}$ (1) and 0.68 and 0.32 for $Ni(chxn)_2Cl_{1.28}Br_{1.72}$ (2), respectively and those at the counter halogen sites are 1.483 and 0.517 for (1) and 0.60 and 1.40 for (2), respectively. Accordingly, their formula can be correctly represented as $[Ni(chxn)_2Cl_{0.976}Br_{0.024}]\ Cl_{1.488}Br_{0.517}$, for (1) and $[Ni(chxn)_2Cl_{0.68}Br_{0.32}]\ Cl_{0.60}Br_{1.40}$ for (2) [11].

In order to discuss their electronic structures, it is essential to decide whether the bridging halogens are located at midpoints between neighboring two Ni atoms (Ni^{III}–X–Ni^{III} structure) or deviated from the midpoints (Ni^{II}...X–Ni^{IV}–X structure). On the basis of the X-ray diffraction, it was concluded that these Ni compounds have the Ni^{III}–X–N^{III} structures. Firstly, their Ni^{III}–X distances are significantly shorter than those of the discrete octahedral Ni^{III} compounds, $[Ni^{III}X_2([14]aneN_4)]ClO_4$ (X = Cl and Br). Secondly, the structure analyses of these compounds do not indicate positional disorders of the bridging halogen atoms. The thermal ellipsoids of the bridging halogen atoms are very small. Finally, neither diffuse scattering nor satellite peak relating to a superstructure has been observed on the X-ray oscillation and Weissenberg photographs of these compounds.

The *b*-axis and *c*-axis are correspondent with the Ni^{III}–X–Ni^{III} distance along the chain and the inter-chain distance in the direction of the hydrogen-bonds, respectively. These two axes are systematically influenced by substitution of the bridging halogens and counteranions. The axes in $Ni(chxn)_2Cl_xBr_y$ increase in the sequence $[Ni(chxn)_2Cl]Cl_2 < [Ni(chxn)_2Cl_{0.976}Br_{0.024}]Cl_{1.483}Br_{0.517} < [Ni(chxn)_2Cl_{0.58}Br_{0.32}]Cl_{0.60}Br_{1.40} < [Ni(chxn)_2Br]Br_2$, due to the increase of the amounts of Br ions with larger ionic radius. Next, in order to investigate the effect of the counteranions of NO_3^- and halogen ions (X^-) on the *b*- and *c*-axes, we compare $[Ni(chxn)_2X](NO_3)_2$ with $[Ni(chxn)_2X]X_2$ (X = Cl and Br). While the Ni^{III}–X or Ni^{III}–X–Ni^{III} distances (*b*-axis) are almost similar in compounds with the same bridging halogens, the *c*-axes of the NO_3^- compounds are much larger than those of X^- compounds, due to the larger ionic radius of NO_3^- compared with those of X^-. The correlation between the *b*-axis and *c*-axis is shown in Fig. 4. The Ni^{III}–X–Ni^{III} distances or *b*-axes are dependent on the species of bridging halogen and almost constant in the same bridging halogens. This is due to the tight covalent bonds of Ni^{III}–X–Ni^{III}. Unfortunately, single crystals of $Ni(chxn)_2X(ClO_4)_2$ (X = Cl and Br) and $Ni(chxn)_2Cl(BF_4)_2$ were not obtained. Therefore, their crystal parameter such as *a*-, *b*- and *c*-axes were obtained by using X-ray powder patterns, since their structures are also isomorphous to $Ni(chxn)_2X_3$ whose crystal structures were determined by single-crystal X-ray diffraction methods. The correlations between *b*- and *c*-axes are also shown in Fig. 4. The lattice constants along the 1-D chains (*b*-axes) in the compounds with the same bridging halogens are almost unchanged, while the *c*-axes or the distances in the direction of the interchain hydrogen-bonds are remarkably lengthened in the counteranion order $X < NO_3 < BF_4 < ClO_4$. Such a trend is consistent with the order of the counteranion ionic radius. Since the Ni^{III}–X–Ni^{III} covalent bonding is tight, the larger counteranions cannot approach to the chains, resulting in lengthening the *c*-axes.

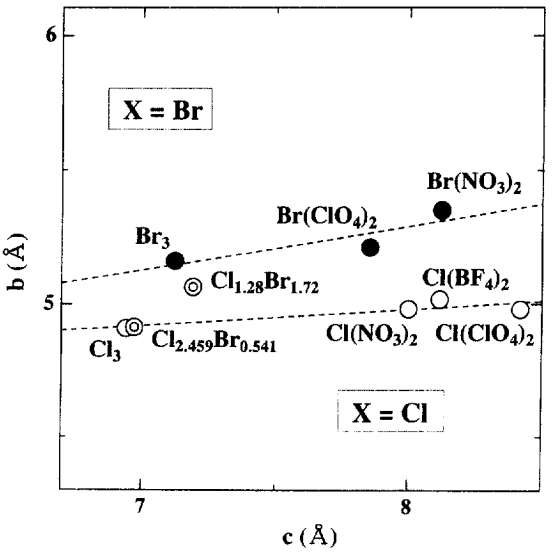

Fig. 4. Correlation between b- and c-axis in $Ni(chxn)_2XY_2$.

At this stage, it is very interesting to compare the correlation between the b- and c-axes in the Ni compounds with those in the Pd and Pt compounds in the $M(chxn)_2ClY_2$ ($Y = Cl^-$ and ClO_4^-), systems where the Ni compounds exhibit Ni^{III} states, and the Pt and Pd compounds exhibit M^{II}–M^{IV} mixed-valence states. The correlation is shown in Fig. 5. Going from $Y = Cl$ to ClO_4 in the Pt compounds, both b- and c-axes are lengthened, while the Pt^{IV}–Cl distances in both compounds are almost constant, and the Pt^{II}...Cl distance in the ClO_4 compound is much longer than that in the Cl compounds [13,14]. The c-axis in the ClO_4 compounds is much larger than that in the Cl compound, due to the difference of their ionic radius and the hydrogen bond systems. A similar trend is also observed in the Pd compounds, but the degree of the inclination is smaller than that of the Pt compounds. Such results are reasonable from the viewpoint of the intervalence interaction. Since the interaction or overlapping of orbitals between Pd^{II} and Pd^{IV} atoms through the bridging halogens is larger, judging from the results of intervalence CT bands and electrical conductivities. The Pd^{II}...Cl–Pd^{IV} distance or b-axis is also short. Since the ClO_4 counteranion cannot approach the chain, the c-axis lengthen compared with the Pt compounds. In the Ni compounds, such trends are even more prominent as shown in Fig. 5, due to the tight covalent bonding of Ni^{III}–Cl–Ni^{III}.

2.3. CP-MAS ^{13}C-NMR of Ni^{III} compounds

CP-MAS ^{13}C-NMR spectra are good probes for evaluating their crystal and electronic structures. The CP-MAS ^{13}C-NMR spectra of $Ni(chxn)_2X_3$ ($X = Cl$, Br and mixed-halides) observed at room temperature exhibited three resonance lines

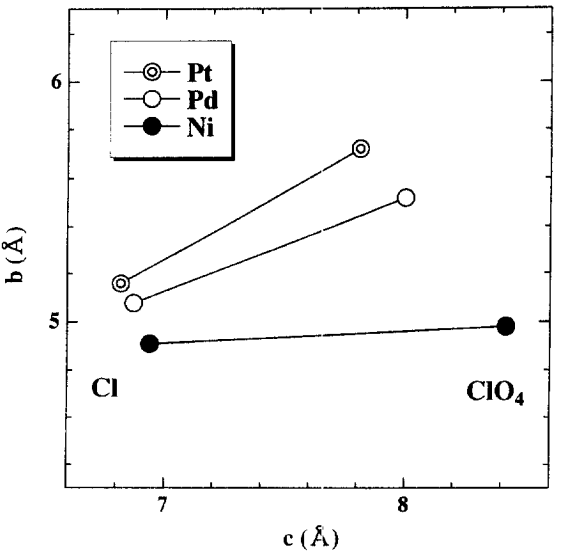

Fig. 5. Correlation between b- and c-axis in $M(chxn)_2ClY_2$ (M = Pt, Pd and Ni; Y = Cl and ClO_4).

with almost equal integrated intensity (Fig. 6). These results are in good agreement with the crystal structural data, revealing the presence of three kinds of crystallographically independent carbon atoms of the chxn ligands in the crystals, namely, α-, β-, and γ-carbons. In contrast with such results, the ^{13}C-NMR spectrum of $[Pd(chxn)_2][PdCl_2(chxn)_2](ClO_4)_4$ exhibits the doublet signal of the α-carbons due to the Pd^{II} and Pd^{IV} components.

2.4. XP spectra and Auger spectra of Ni^{III} compounds

In order to estimate the on-site Coulomb energies of these compounds, their Auger spectra and XP spectra were measured [15,16]. Fig. 7 shows the valence-band XP spectra of the Ni compounds, which were obtained by using Mg–K_α radiation. Broad peaks centered at 3–4 eV binding energies are observed. Both Ni 3d and bridging halogen 3p(Cl) or 4p(Br) electrons will contribute to the XPS intensities in this region. Since the XPS cross section of the Ni 3d electrons is comparatively larger than those of Cl 3p and Br 4p electrons for Mg–K_α radiation, the broad peak at 3–4 eV can be considered to have dominant 3d character. The Ni 2p XP spectra obtained using Mg–K_α radiation are shown in Fig. 8. The spectra are composed of two peaks, Ni $2p_{3/2}$ and Ni $2p_{1/2}$, where the former is observed at higher energy compared with the latter. These binding energies are higher than those in Ni^{II} complexes. Fig. 9 shows the Auger spectra which are obtained with Al–K_α radiation, since the strong N 1s XP line appears in the Auger spectral region with excitation of the Mg–K_α radiation. From these results, the U values are obtained by using the equation described previously [15,16]. All results are listed in Table 2. The U in these compounds are about 5 eV.

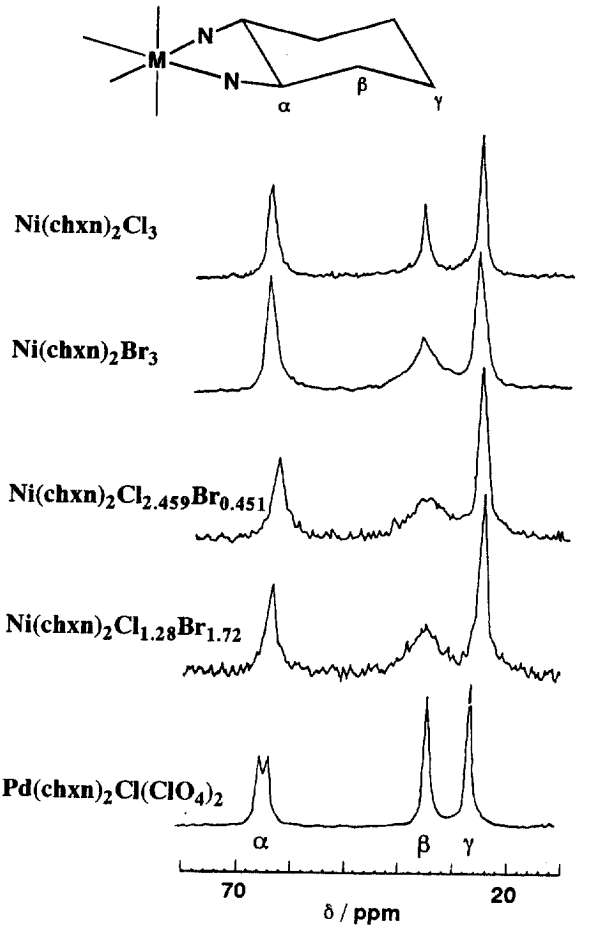

Fig. 6. CP-MAS ^{13}C-NMR spectra of $Ni(chxn)_2X_2$ and $Pd(chxn)_2Cl(ClO_4)_2$.

2.5. *Absorption spectra of Ni^{III} compounds*

The optical conductivity spectra of the single crystals of these compounds are shown in Fig. 10. They were obtained by the Kramers–Kronig transformation from the polarized reflectivity spectra with the electric vector E parallel to the chain axis b ($E \| b$). In the energy region from 1.2 to 2.0 eV, prominent absorptions are observed polarized parallel to the chain axis b, but no prominent structures are observed for the E⊥b spectra (Table 2). As mentioned above, the on-site Coulomb energies are estimated to be about 5 eV. On the other hand, the lowest transitions are observed in the energy regions from 1.2 to 2.0 eV. Therefore, the lowest transitions are considered as those of the bridging halogens to the upper-Hubbard bands of Ni $3d^2_{\bar{z}}$. These compounds are then, not Mott-insulators, but CT-insula-

tors, where the energy levels of the bridging halogens are located between the lower and upper Hubbard bands composed of the Ni^{III} $3d_{z^2}^2$ orbitals. The peak energies shift in the order $Ni(chxn)_2Cl_3 > Ni(chxn)_2Cl_{2.459}Br_{0.0541} > Ni(chxn)_2Cl_{1.28}Br_{1.72} > Ni(chxn)_2Br_3$, which is understood in terms of energy difference of the 3p of Cl and 4p of Br ions. In compounds with the same bridging halogens, the peak energies of the NO_3^- compounds are higher than those of the halogen-counteranions, due to a little longer Ni^{III}–X–Ni^{III} distances in the NO_3^- compounds.

2.6. *Electrical conductivities of Ni^{III} compounds*

Single crystal electrical conductivities have been measured along the chain axes by the four-probe method (Fig. 11). All these compounds show semiconducting behavior. The activation energies (E_a) and the conductivities at room temperature (σ_{RT}) are listed in Table 2, where the resistivities at room temperature and the activation energies increase in the order $Ni(chxn)_2Br_3 < Ni(chxn)_2Cl_{1.28}Br_{1.72} < (Ni(chxn)_2Cl_{2.459}Br_{0.541}) < Ni(chxn)_2Cl_3$, and in the same bridging halogens those

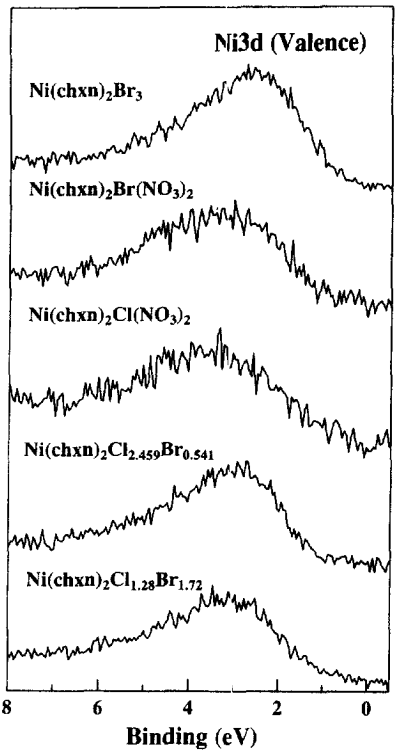

Fig. 7. Valence-band XP spectra of $Ni(chxn)_2XY_2$.

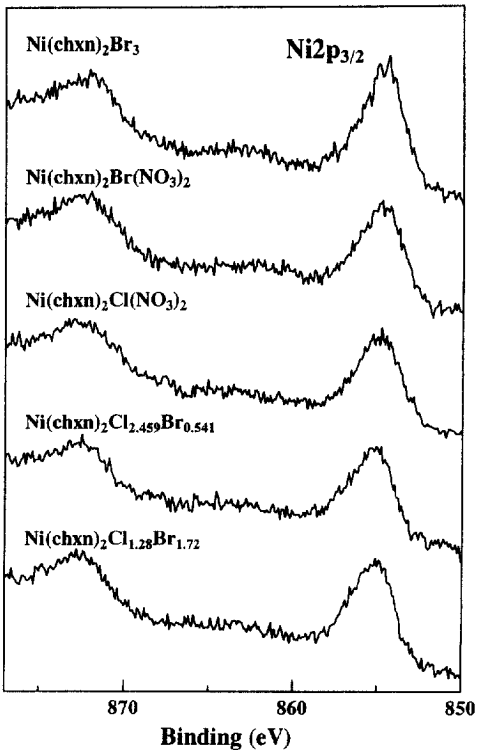

Fig. 8. Ni 2p XP spectra of $Ni(chxn)_2Y_2$.

of the NO_3^- compounds are larger than those of halogen–counteranion compounds. Such orders are the same as those of the peak energies of the charge transfer bands.

2.7. Magnetic susceptibilities of Ni^{III} compounds

The temperature-dependent magnetic susceptibility measurements reveal that all these compounds show the very strong antiferromagnetic interactions, due to the superexchange mechanism through the bridging halogens between neighboring spins located on the Ni $3d_{z^2}^2$ (Fig. 12).

3. Competition between charge density wave and spin density wave states in Ni-Pd mixed-metal complexes

The $[Ni(chxn)_2Br]Br_2$ (SDW) and $[Pd(chxn)_2][Pd(chxn)_2Br_2]Br_4$ (hereafter abbreviated as $Pd(chxn)_2Br_3$, CDW) are isomorphous with each other (same space group I222), although the positions of the bridging halogens are different from each other,

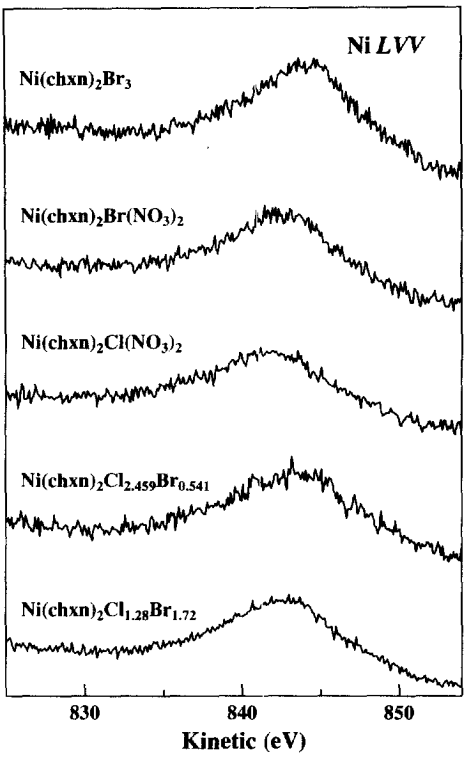

Fig. 9. Ni LVV Auger spectra of $Ni(chxn)_2XY_2$. The LVV means a radiation of a valence electron when other valence electron falls down to the vacant L shell of Ni.

that is, located at midpoints and distorted from the midpoints between neighboring two metal ions, respectively, as mentioned above. If we can obtain single crystals of the Ni–Pd mixed-metal compounds, we can directly investigate the competition between the electron-correlation (U) in Ni^{III} states (SDW) and the electron-phonon-interaction (S) in the Pd^{II}–Pd^{IV} mixed-valence states (CDW) in this system. In

Table 2
Electron-correlations (U), CT peak energies (E_{CT}), activation energies (E_a), and electrical conductivities at room temperature ($\log \sigma$)

	U (eV)	E_{CT} (eV)	E_a (eV)	$\log \sigma$ (s cm^{-1})
$Ni(chxn)_2Cl(NO_3)_2$	~4.47	1.95	0.302	−6.61
$Ni(chxn)_2Cl_3$	~4.9	1.80	0.232	−6.00
$Ni(chxn)_2Cl_{2.459}Br_{0.541}$	~5.95	1.75	[a]	[a]
$Ni(chxn)_2Br(NO_3)_2$	~5.91	1.45	0.178	−5.61
$Ni(chxn)_2Cl_{1.28}Br_{1.72}$	~535	1.45	0.137	−4.73
$Ni(chxn)_2Br_3$	~5.84	1.28	0.117	−3.16

[a] Single crystals are too small to be measured.

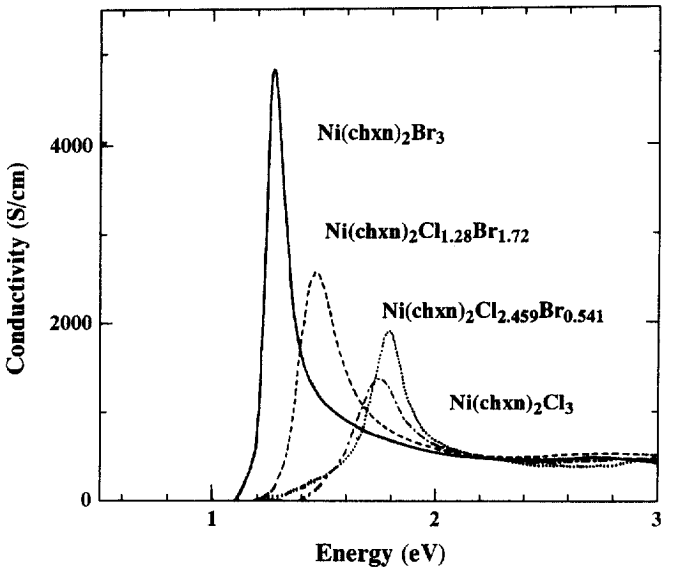

Fig. 10. Optical conductivity spectra of single crystals of $Ni(chxn)_2XY_2$.

studies on the transition metal oxides, the filling control or doping method is usually employed, where the physical parameters are controlled indirectly. On the other hand, in the MX-chain compounds, we can control the physical parameters directly by substituting the chemical factors such as metal ions, bridging halogens, etc.

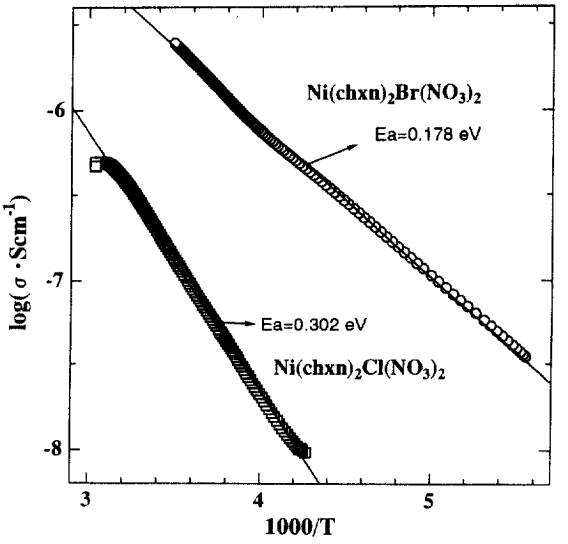

Fig. 11. Single-crystal electrical conductivities of $[Ni(chxn)_2X](NO_3)_2$.

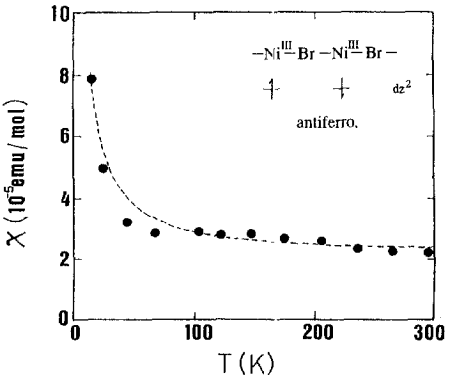

Fig. 12. Magnetic susceptibilities of $[Ni(chxn)_2Br]Br_2$.

According to such a strategy, the physical properties of a series of $Ni_{1-x}Pd_x(chxn)_2B_3$ with various mixing ratios were investigated [17,18].

3.1. Syntheses of $Ni_{1-x}Pd_x(chxn)_2Br_3$

A series of single-crystals of the Ni–Pd mixed-metal compounds, $Ni_{1-x}Pd_x(chxn)_2B_3$ were obtained by electrochemical oxidation methods of the mixed methanol solutions of $[Ni(chxn)_2]Br_2$ and $[Pd(chxn)_2]Br_2$ with various mixing ratios. As electrolyte, tetra-n-butylammonium bromide was used. The current dependence and concentration dependence on the ratios of the Pd and Ni ions in these compounds were investigated. The ratios between the Pd and Ni ions for all compounds were determined by ICP emission spectrometry.

3.2. Crystal structures of $Ni_{1-x}Pd_x(chxn)_2Br_3$

Since the crystal structures of $Ni_{1-x}Pd_x(chxn)_2Br_3$ could not be determined by single crystal four-circle X-ray diffractometry; only their crystal parameters such as *a*, *b* and *c* axes were obtained. The crystal structures of $Ni_{1-x}Pd_x(chxn)_2B_3$ are isomorphous to $[Ni^{III}(chxn)_2Br]Br_2$ and $Pd(chxn)_2B_3$, although the positions of the bridging halogens are assumed to be different among these compounds. Accordingly, their structures are assumed as follows. The four N atoms of two chxn ligands are coordinated to Ni and Pd atoms in a planar fashion. The $M(chxn)_2$ moieties, lying on special position 222, are bridged by halogen atoms and stacked along the *b*-axis, constructing linear-chain structures. The neighboring $M(chxn)_2$ moieties along the chain are linked by the hydrogen bonds between aminohydrogens and counteranions. Moreover, there are hydrogen bonds among the neighboring chains, constructing two-dimensional hydrogen bond networks parallel to the bc plane. The M–M distances correspond to the *b*-axis. The M–M distances

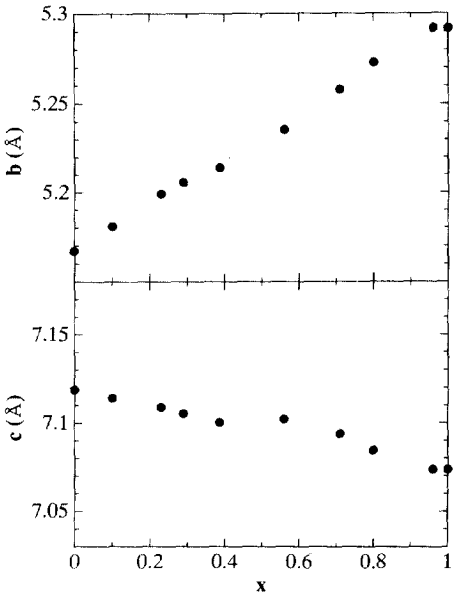

Fig. 13. *b*- (upper) and *c*-axes (lower) in $Ni_{1-x}Pd_x(chxn)_2Br_3$.

(*b*-axis) increase in Pd component due to the larger ionic radius of a Pd ion, compared with that of a Ni ion as shown in Fig. 13. On the other hand, the *c*-axis which is along the direction of the inter-chain hydrogen-bonds gradually decreases with increase of the Pd ratios, since the counter Br^- ions can approach the chain. Such a negative correlation is also observed in $M(chxn)_2XY_2$ (X = Cl and Br; $Y = ClO_4$ and X).

3.3. IR and Raman spectra of $Ni_{1-x}Pd_x(chxn)_2Br_3$

In this system, the IR ν(N-H) signals around 3000 cm^{-1} are very good probes for evaluating their oxidation states [19]. The $[Ni(chxn)_2Br]Br_2$ shows a singlet ν(N–H) signal around 3000 cm^{-1} due to the Ni^{III} oxidation state, while the $Pd(chxn)_2B_3$ shows doublet ν(N–H) signals due to the Pd^{II} and Pd^{IV}, oxidation states. Fig. 14 shows the IR spectra of $Ni_{1-x}Pd_x(chxn)_2B_3$ at 17 K. The compounds with x larger than ca. 0.5 show triplet signals which are assignable to the superpositions of the Pd^{II}–Pd^{IV} doublet state and the Ni^{III} singlet state. The doublet peaks of ν(N–H) attributable to the Pd^{II} and Pd^{IV} sites approach each other with increase of the Ni component. Compounds with x smaller than ca. 0.5 show the singlet ν(N-H) signal, indicating that in this system the oxidation states of Pd^{II}–Pd^{IV} mixed-valence states approach Pd^{II} states with increase of the Ni component.

The Raman spectrum is another good probe for evaluating their oxidation states. Clark and Swanson have both measured Raman spectra for many M^{II}–M^{IV}

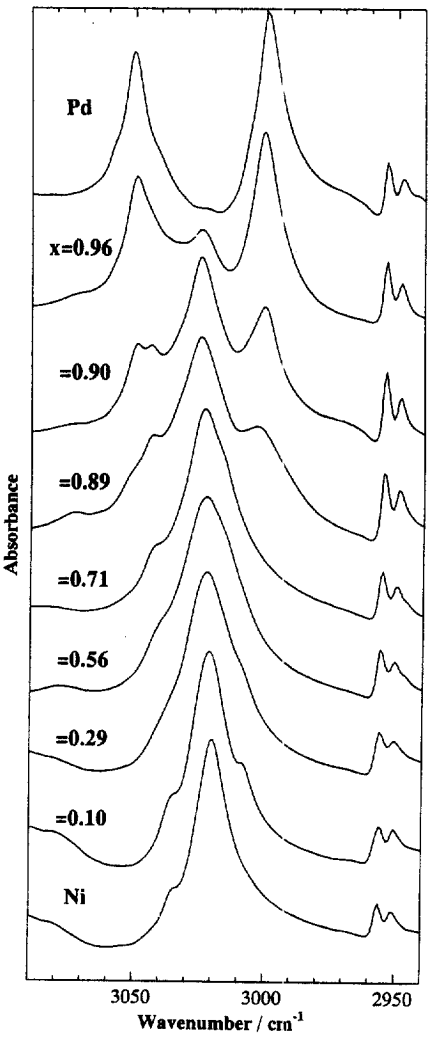

Fig. 14. IR spectra of ν(N-H) in $Ni_{1-x}Pd_x(chxn)_2Br_3$.

mixed-valence compounds [2,4]. The numbers and intensities of Raman spectra depend on their oxidation states in these systems. Fig. 15 shows the Raman spectra of the Ni–Pd mixed-metal compounds along with those of the pure Ni^{III} and pure Pd^{II}–Pd^{IV} mixed-valence compounds. The pure Pd^{II}–Pd^{IV} mixed-valence compound, $Pd(chxn)_2B_3$, shows characteristic overtone progressions of $\nu(Pd^{IV}-Br)$ in the Raman spectrum, while the pure Ni^{III} compound, $[Ni(chxn)_2Br]Br_2$ shows no Raman signals because of the central positions of bridging Br ions between neighboring two Ni^{III} atoms. The intensities are weakened and the number of

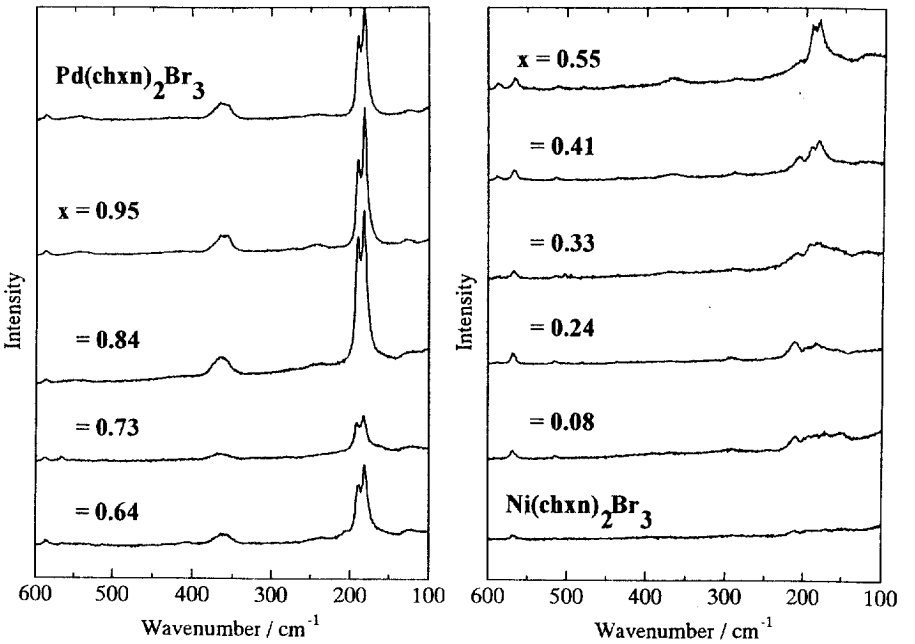

Fig. 15. Resonance Raman spectra of $Ni_{1-x}Pd_x(chxn)_2Br_3$.

overtones decrease with increase of the Ni component, indicating that the bridging Br^- ions positions gradually shift to the central positions from the distorted positions with decrease of the Pd component. These results indicate that the oxidation states of the Pd^{II}–Pd^{IV} mixed-valence states approach Pd^{III} with increasing Ni component. The results are consistent with the IR spectra mentioned above.

3.4. XP spectra and Auger spectra of $Ni_{1-x}Pd_x(chxn)_2Br_3$

In order to directly investigate their oxidation states, the XP and Auger spectra were measured for these compounds at 165 K. Fig. 16 shows that Ni $2p_{3/2}$ and Ni $2p_{1/2}$ signals in the XP spectra of the Ni components of the Ni–Pd mixed-metal compounds are essentially the same in these compounds, indicating that the Ni ion oxidaton states are +3 in all these compounds. On the other hand, the $Pd3d_{5/2}$ and $Pd3d_{3/2}$ signal of the Pd components of the Ni–Pd mixed-metal compounds gradually change from relatively broad to sharp. The spectra are resolved into the Pd^{II} and Pd^{IV} components as shown in Fig. 17, where the Pd^{II} and Pd^{IV} species gradually approach each other with decrease of Pd component. As shown in Fig. 16, the binding energy differences between the Pd^{II} and Pd^{IV} components gradually decrease with decrease of the Pd component, indicating that the Pd^{II}–Pd^{IV} mixed-valence states gradually approach the Pd^{III} state. These results are consistent with

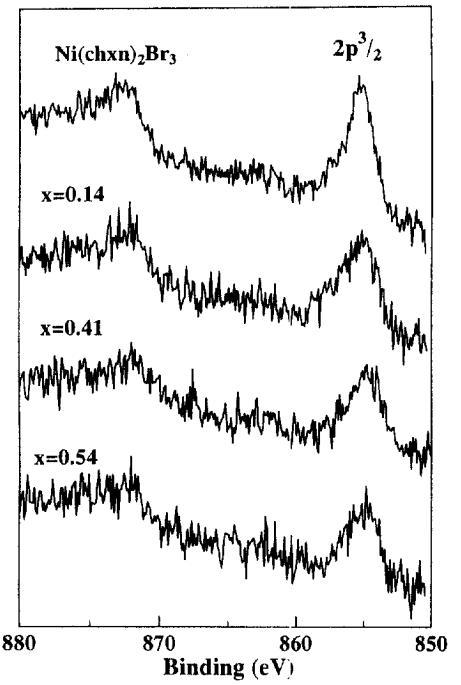

Fig. 16. XP spectra of Ni components in $Ni_{1-x}Pd_x(chxn)_2Br_3$.

those of the IR and resonance Raman spectra, and reveal that the electron–phonon interactions in the Pd^{II}–Pd^{IV} mixed-valence states is weakened with increase in the Ni^{III} components which have strong electron correlation. The magnitude of the Ni ions electron correlation in these Ni–Pd mixed metal compounds is estimated to be 4–5 eV by XP and Auger spectra. On the other hand, the electron–phonon interaction of the Pd^{II}–Pd^{IV} mixed-valence state is estimated to be about 1 eV. The experimental results are fully consistent with these physical parameters.

3.5. Magnetic properties of $Ni_{1-x}Pd_x(chxn)_2Br_3$

In order to investigate the magnetic properties of these compounds, temperature-dependent EPR and magnetic susceptibilities are measured. The magnetic susceptibility of the pure Ni^{III} compound, $[Ni(chxn)_2Br]Br_2$ is small and almost temperature-independent from room to low temperature as shown in Fig. 12. This is due to the very strong antiferromagnetic interaction among the spins located on the Ni $3d_{z^2}$ orbitals via the bridging halogen ions. At very low temperature, the magnetic susceptibility increases abruptly. Such a component obeys the Curie law, which is considered to be due to the impurities of the chain edges and defects. The

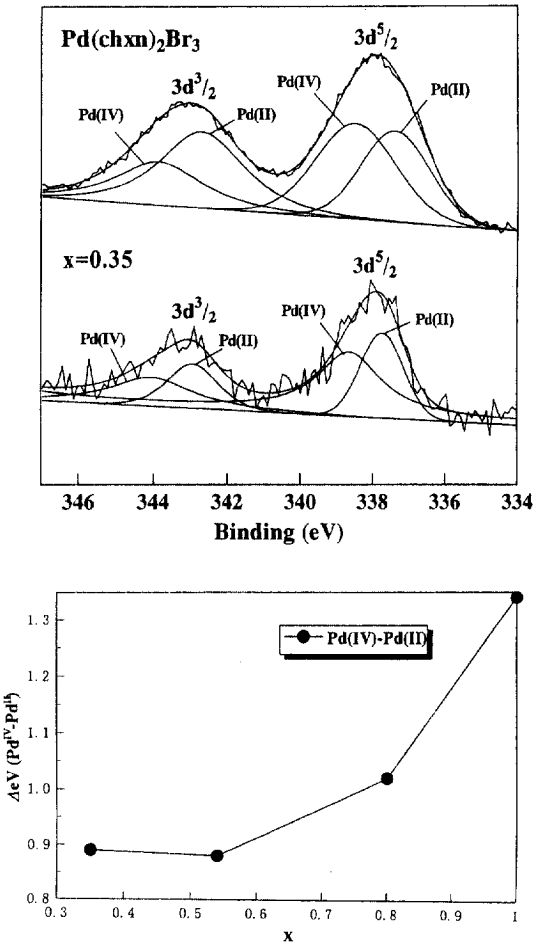

Fig. 17. XP spectra of Pd components (upper) and differences of binding energies between Pd^{II} and Pd^{IV} components (lower) in $Ni_{1-x}Pd_x(chxn)_2Br_3$.

pure Pd^{II}–Pd^{IV} mixed-valence compound, $Pd(chxn)_2Br_3$ is diamagnetic. In this compound, an abrupt increase in susceptibility is also observed at very low temperature, and is also due to Pd^{III} impurities at chain edges or defects; it obeys the Curie law. In the Ni–Pd mixed-metal compounds, the absolute values of the magnetic susceptibilities gradually decrease with increase of the Pd component.

In the EPR spectra at room temperature, the pure Ni compound shows a very broad signal around $g = 2$, due to the very strong antiferromagnetic interaction among spins located in the Ni $3d_{z^2}$ orbitals. The signals sharpened gradually with increase of the Pd component (Fig. 18). The integrated intensities plotted against the Pd components obtained by Kuroda and Marumoto are shown in Fig. 19.

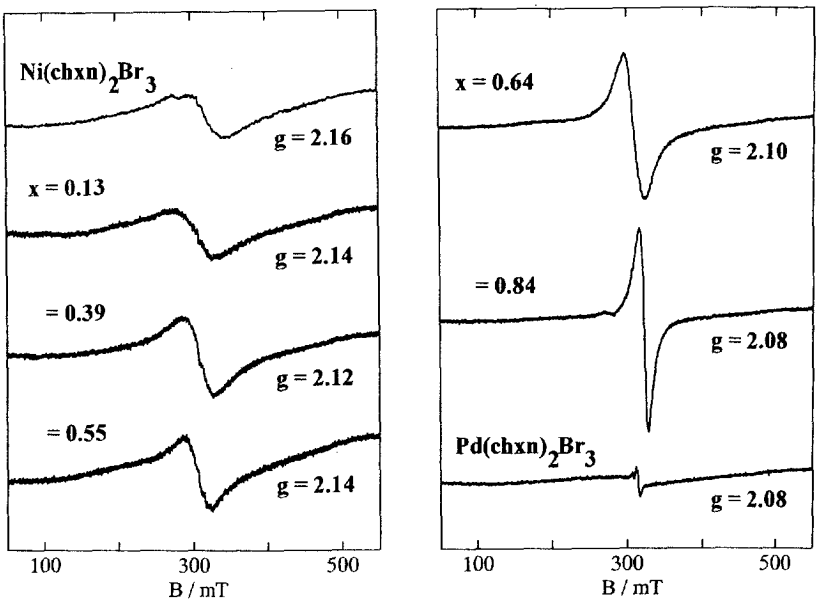

Fig. 18. EPR spectra of $Ni_{1-x}Pd_x(chxn)_2Br_3$.

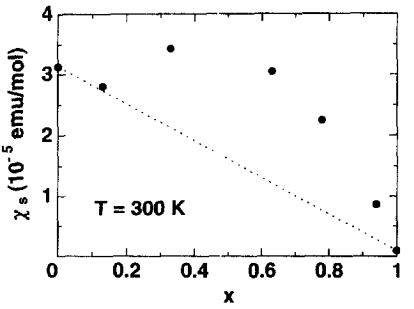

Fig. 19. Dependence of spin susceptibilities at room temperature of $Ni_{1-x}Pd_x(chxn)_2Br_3$ obtained by EPR signals.

The dotted line shows the summation of Ni^{III} and Pd^{II}–Pd^{IV} components. The results are not linear but deviate to the upper side [20]. Showing that the Pd oxidation state approaches Pd^{III} with increase of the Ni component.

4. Conclusion

A series of Ni^{III} complexes were synthesized. They are CT-insulators and their electronic structures are tuned by substituting the bridging halogens and the

counteranions. The Ni–Pd mixed metal compounds, $Ni_{1-x}Pd_x(chxn)_2Br_3$ were synthesized, where the electron-correlation in the Ni sites and the electron–phonon interaction in the Pd sites compete with each other. The Pd^{II}–Pd^{IV} mixed-valence states approach Pd^{III} with increase of the Ni component due to the very strong electron-correlation of the Ni sites.

Acknowledgements

We are grateful to Professors N. Kuroda, Y. Wada, T. Mitani, Y. Iwasa, R. Ikeda, T. Kobayashi, K. Nasu, K. Iwano, K. Toriumi, H. Miyamae, K. Marumoto, S. Kuroda, and T. Koda for their collaboration and many enlightening discussions. This work was supported by a Grant-in-Aid for Scientific Research from the Ministry of the Education, Science and Culture of Japan, Casio Science Promotion Foundation, Ito Science Foundation, Inoue Science Foundation, The Sumitomo Foundation, The Japan Securities Scholarship Foundation, Mitsubishi Foundation, Nageya University Foundation, Daiko Foundation, Yoshida Foundation for Science and Technology, Ciba–Geigy Foundation for the Promotion of Science, The Mazda Foundation's Research Grant, Tokai Foundation for Science and Technology, and Kumagai Foundation for Science and Technology.

References

[1] (a) M.B. Robin, P. Day, Adv. Inorg. Radiochem. 10 (1967) 247. (b) J.S. Miller (Ed.), Extended Linear Chain Compounds, vols. I–III, Plenum, New York, 1982.
[2] A.R. Bishop, B.I. Swanson, Los Alamos Sci. 21 (1993) 133.
[3] M. Yamashita, New development in quasi-one-dimensional halogen-bridged metal compounds, in: T. Tsuruta, M. Doyama, M. Seno (Eds.), New Functional Materials, Volume C, Synthetic Process and Control of Functionality Materials, Elsevier, Amsterdam, 1993, p. 539.
[4] R.J.H. Clark, Adv. Infrared Raman Spectrosc. 11 (1983) 95.
[5] K. Nasu, J. Phys. Soc. Jpn. 52 (1983) 3865.
[6] K. Nasu, J. Phys. Soc. Jpn. 53 (1984) 302.
[7] K. Nasu, J. Phys. Soc. Jpn. 53 (1984) 427.
[8] K. Toriumi, Y. Wada, T. Mitani, S. Bandow, M. Yamashita, Y. Fujii, J. Am. Chem. Soc. 111 (1989) 2341.
[9] K. Toriumi, H. Okamoto, T. Mitani, S. Bandow, M. Yamashita, Y. Wada, Y. Fujii, R.J.H. Clark, D.J. Michael, A.J. Edward. D. Watkin, M. Kurmoo, P. Day, Mol. Cryst. Liq. Cryst. 181 (1990) 333.
[10] H. Okamoto, M. Yamashita, Bull. Chem. Soc. Jpn. 71 (1998) 2023.
[11] M. Yamashita, E. Tsuruta, K. Inoue, T. Furuta, H. Okamoto, T. Mitani, K. Toriumi, H. Ohki, R. Ikeda, Synth. Met. 57 (1993) 3461.
[12] M. Yamashita, K. Inoue, T. Tsuruta, A. Ichikawa, H. Okamoto, N. Kimura, H. Ohki, R. Ikeda, H. Kitagawa, S. Bandow, K. Toriumi, T. Mitani, T. Ohishi, H. Miyamae, Mol. Cryst. Liq. Cryst. 256 (1994) 179.
[13] K.P. Larsen, H. Toftlund, Acta Chem. Scand. 31 (1977) 182.
[14] Y. Wada, U. Lemmer, E.O. Gobel, M. Yamashita, K. Toriumi, Phys. Rev. B 52 (1995) 8276.
[15] H. Okamoto, Y. Shimada, Y. Oka, A. Chainani, T. Takahashi, H. Kitagawa, T. Mitani, K. Toriumi, K. Inoue, T. Manabe, M. Yamashita, Phys. Rev. B 54 (1996) 8438.

[16] H. Okamoto, A. Chainani, T. Takahashi, H. Kitagawa, T. Mitani, T. Manabe, M. Yamashita, Synth. Met. 86 (1997) 2139.
[17] T. Manabe, T. Kawashima, M. Yamashita, H. Okamoto, H. Kitagawa, T. Mitani, M. Inokuchi, K. Yakushi, Synth. Met. 86 (1997) 2233.
[18] T. Manabe, M. Yamashita, T. Kawashima, H. Okamoto, H. Kitagawa, T. Mitani, K. Toriumi, H. Miyamae, K. Inoue, K. Yakushi, Opt Probes Conjug. Polym. 3145 (1997) 106.
[19] K. Okaniwa, H. Okamoto, T. Mitani, K. Toriumi, M. Yamashita, J. Phys. Soc. Jpn. 60 (1990) 997.
[20] S. Kuroda, K. Marumoto, T. Manabe, M. Yamashita, Synth. Met., in press.